

Application of FE approach to deformation analysis of RC elements under direct tension

Ronaldas Jakubovskis¹, Rimantas Kupliauskas², Arvydas Rimkus^{1,3} and Viktor Gribniak*¹

¹Laboratory of Innovative Building Structures, Vilnius Gediminas Technical University (VGTU), Sauletekio av. 11, Vilnius LT-10223, Lithuania

²Department of Storm-Water Network, Grinda Ltd., Eiguliu str. 32, Vilnius LT-03150, Lithuania

³Laboratory of Composite Materials, VGTU, Vilnius, Lithuania

(Received February 19, 2018, Revised September 12, 2018, Accepted September 18, 2018)

Abstract. Heterogeneous structure and, particularly, low resistance to tension stresses leads to different mechanical properties of the concrete in different loading situations. To solve this problem, the tension zone of concrete elements is reinforced. Development of the cracks, however, becomes even more complicated in the presence of bar reinforcement. Direct tension test is the common layout for analyzing mechanical properties of reinforced concrete. This study investigates scatter of the test results related with arrangement of bar reinforcement. It employs results of six elements with square 60×60 mm cross-section reinforced with one or four 5 mm bars. Differently to the common research practice (limited to the average deformation response), this study presents recordings of numerous strain gauges, which allows to monitor/assess evolution of the deformations during the test. A simple procedure for variation assessment of elasticity modulus of the concrete is proposed. The variation analysis reveals different deformation behavior of the concrete in the prisms with different distribution of the reinforcement bars. Application of finite element approach to carefully collected experimental data has revealed the effects, which were neglected during the test results interpretation stage.

Keywords: reinforced concrete; heterogeneous material; tension tests; numerical modeling; stochastic effects; arrangement of reinforcement; deformations

1. Introduction

Cracking is a highly complex physical process intrinsic to the concrete. Development of the cracks, which was initiated at the fine, microstructural level, often becomes evident only at the mezostructural range (Tijssens *et al.* 2001, Chen *et al.* 2016). Concrete structure at different scale (Fig. 1) might be considered as a combination of components, which mechanical characteristics and interaction mechanisms are responsible for heterogeneity of the physical properties of the concrete composite. Various defects, inherent to the concrete structure at all consideration levels, could be identified as another important source of the material heterogeneity. The defects appear not only due to mechanical loading: the concrete production process (quality of aggregates, mixture proportions, mixing and transportation technology, pouring errors) is also responsible for the presence of the structural imperfections.

Cracks in the concrete propagate by following the complex topology of the internal structure. Fig. 2 illustrates the cracking process (Chiaia *et al.* 1998, Diamond 2004, Elaqr *et al.* 2007). Under loading, the structural defects appeared at the pre-loading stage are growing and form macrocracks, which topology follows the tensile stresses

layout. This process is closely related with distribution and mechanical characteristics of the coarse aggregates. Particularly, the crack growth is under control of topology of the interfacial transition zone that is, in principle, a most vulnerable component of the concrete structure (Chiaia *et al.* 1998). Research works conducted by Van Mier in co-authorship (Van Mier 1991, Schlangen and Van Mier 1992, Chiaia *et al.* 1998, Van Mier and Van Vliet 2003, Prado and Van Mier 2003, Shiotania *et al.* 2003, Caduff and Van Mier 2010, Man and Van Mier 2011) should be mentioned in this regard. These works have stipulated the inference that relative size (in respect to dimension of the specimen) and distribution of the aggregates are the most important characteristics responsible for the scatter of the test outputs. The distribution of aggregates is closely related with the mix design and the production technology (including number of rotation and rotation speed of the mixer, pouring position and specimen layout, and concrete vibration intensity).

The heterogeneous structure determines different mechanical properties of the concrete in different loading situations. It could be related with a low resistance of the concrete matrix to development of the tension cracks. This property causes a brittle failure character and a very low tensile strength of the concrete (in comparison with the other major mechanical properties of the material). In practice, the tension zone of concrete elements is reinforced for compensating the low cracking resistance. Steel bars with different surface shape is the commonly used type of the reinforcement (Clark 1946). In the presence of bar

*Corresponding author, Ph.D.
E-mail: Viktor.Gribniak@vgtu.lt

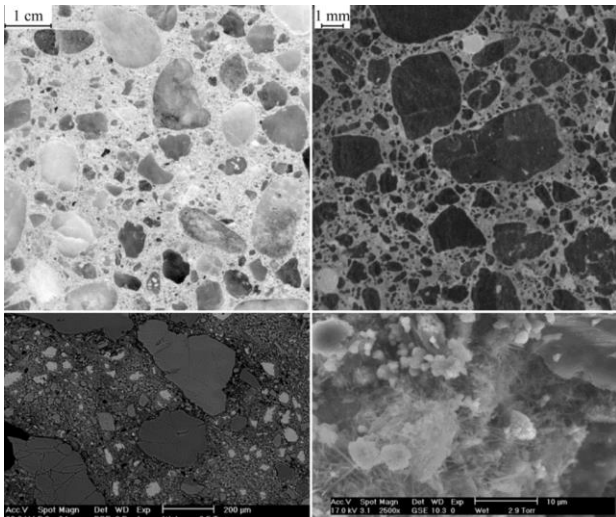


Fig. 1 Different levels of heterogeneity of concrete structure (Tijssens *et al.* 2001)

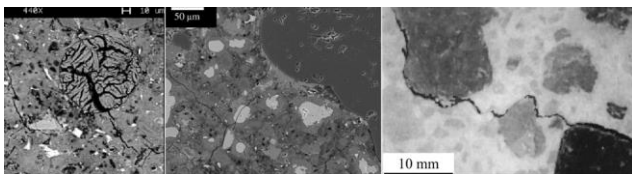


Fig. 2 Cracking of concrete: nano-cracking (Diamond 2004), micro-cracking (Elaqra *et al.* 2007), and mezo-cracking (Chiaia *et al.* 1998)

reinforcement, however, development of the cracks becomes even more complicated due to appearance of a new structure component – the interaction zone between the concrete and reinforcement (Mang *et al.* 2016).

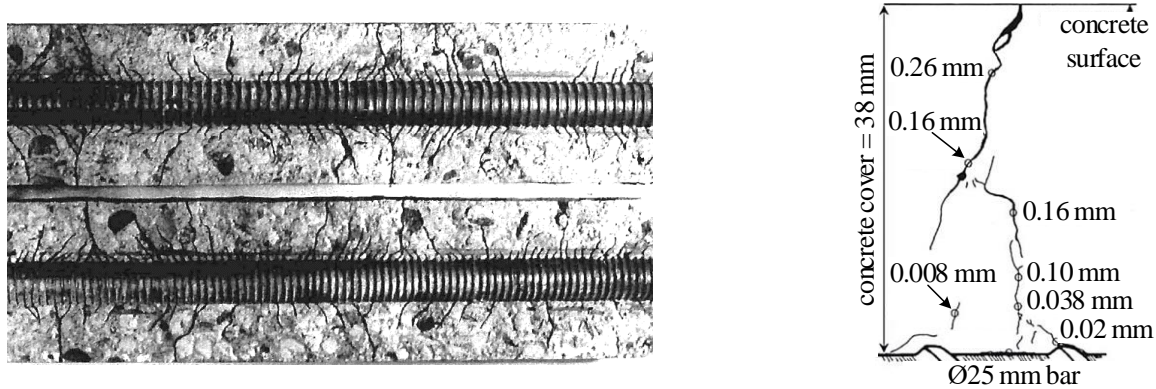
The reinforcement enables transferring the tensile stresses through the crack plane making possible development of the multiple cracks in the tensile concrete. At a certain distance from the transverse crack, the concrete continues carrying tensile stresses because of the bond mechanism. Goto (1971) related this process with the formation of secondary cracks (Fig. 3(a)) caused by the transfer of bond stresses to the surrounding concrete between the transverse primary cracks. Broms (1965) has characterized two types of cracks with different geometry. One type is the primary visible crack attaining the concrete surface, while the secondary cracks do not progress up to the concrete surface. The crack initiation could be also related with the restrained shrinkage effect (Gribniak *et al.* 2013b): the stiff reinforcement induces tension stresses in the concrete by resisting its shrinkage deformations.

As can be observed in Fig. 3(b), the crack width varies with the distance to the reinforcement bar. Despite the high amount of experimental and theoretical investigations carried out during the last century, a direct relationship between crack widths at the surface and inside the concrete (close to the bar) has not been determined (Beeby 1978). There is also no general agreement on the area of the effective concrete in tension. Specimens with different dimensions are used for representing the behavior of structural elements, which naturally increases the scatter of

the test results, reducing the reliability of the assessed responses (Lee and Kim 2009, Gribniak *et al.* 2015). One of the most widely used layouts representing structural response of reinforced concrete is the direct tension test. A concrete prism reinforced with a bar in the center is the common test specimen for the analysis. During the test, the reinforcing bar is fixed by the grips of the testing machine and the test is performed under displacement or force control (Ingaffea *et al.* 1984). Despite the apparent simplicity of the tensile test setup, interpretation of the test results might be inadequate: the experimental evidence often disagrees with the general assumption of similarity between average strains of the reinforcement and concrete. In general, the total area of the concrete is assumed effective in tension though this assumption is adequate only for limited concrete cover ranges (Gribniak *et al.* 2017).

Test results obtained by the authors (Gudonis *et al.* 2014, Jakubovskis *et al.* 2014, Gribniak *et al.* 2016a) and other researchers, e.g., Broms and Lutz (1965), Borosnyói and Snóbli (2010), Caldentey *et al.* (2013), indicated that the cracking pattern is dependent on the geometry of the specimen and the arrangement of the reinforcement. Rostásy *et al.* (1976), Hwang (1983), Williams (1986), and Purainer (2005) have demonstrated experimentally that distributing the same reinforcement area in a higher number of smaller diameter bars may increase the stiffness of concrete ties. Such an increase might be a consequence of two effects. On the one hand, an increase in the total bond area increases the bond capacity to release the extra fracture energy during the crack formation stage. On the other hand, the confinement of the intact concrete between the closely spaced bars constrains the internal cracks. The test data reported by Broms and Lutz (1965) supports the latter inference. It has been shown (Fig. 4(a)) that the number of cracks between the closely distributed bars might significantly exceed the number of cracks in other areas of the concrete. Otsuka and Ozaka (1992) supported this deduction by reducing the distance between the reinforcement bars pulled-out from a massive concrete block (Fig. 4(b)). Using test results of ties with different reinforcement and testing layouts, Rimkus *et al.* (2017) revealed that differences in the crack spacing are dependent on the concrete cover.

Analysis of the internal cracking (and strain distribution) is even too complicated to be performed experimentally. A finite element approach can be used to solve this problem. In last decades, numerical simulations were used for analysis of different aspects of the structural behavior: crack propagation (Theiner and Hofstetter 2009, Patel *et al.* 2016), deformation problems (Gribniak *et al.* 2013a), and bond behavior (Jendele and Cervenka 2006). Fig. 5 presents an example of an elaborate analysis of the deformation behavior of RC tie performed by Gribniak *et al.* (2017). To investigate deformation state of the concrete, the boundary segments of two (60×60×640 mm and 100×100×640 mm) concrete prisms reinforced with 10 mm bar were modeled. The FE software ATENA was used for this purpose. Accounting for the symmetry conditions, quarter-segments were considered. Due to the limited computation capacity, two different meshes were generated: the quarter-segments



(a) Crack patterns around 32 mm bar with different rib spacing (Goto 1971) (b) Experimental crack width variation in the cover concrete (Borosnyói and Snóbli 2010)

Fig. 3 Cracking of the reinforced concrete

of $60 \times 60 \times 640$ mm (Fig. 5(a)) and $100 \times 100 \times 640$ mm (Fig. 5(b)) prisms were modeled using 3 mm and 5 mm tetrahedral finite elements, respectively. The triple refinement was used to represent the reinforcement and concrete contact zone. The respective models contain about 100,000 and 60,000 finite elements in total. The softening law proposed by Hordijk (1991) was assumed to describe cracking of the concrete. The contact between the reinforcement and concrete was modeled using the ribbed bond model proposed by Michou *et al.* (2015). These results indicate evident increase of the strain gradient in the concrete with increase of the cover. The considered models, however, were composed neglecting the aforementioned heterogeneity of the concrete structure.

This study is dedicated to analysis of the scatter of test results of RC ties subjected to short-term loading focusing the components, which are related with the material heterogeneity and reinforcement layout. The test results of the extensive test program performed by the second author are used for the evaluation. Specific testing methodology enabled collecting test data (deformation sets) representative for the scatter analysis. A simple procedure for assessment of variation of the material characteristics (the deformation modulus of concrete) has been proposed. Particular deformation behavior of the ties is analyzed by applying FE approach. Unlike the common practice, numerical models account for the restrained shrinkage effect at the pre-loading stage. The numerical visualization has evidenced the effects neglected during the test results interpretation stage. The simulations have also proved versatility of the fundamental modelling principles for analysis of specific aspects of the experimental behavior.

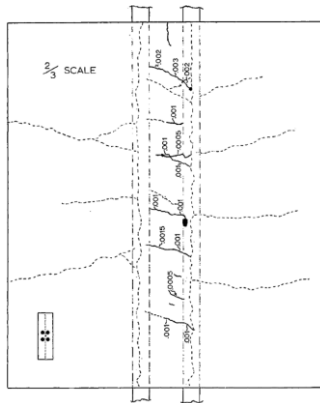
2. Experimental program

This study is based on the test results obtained by the second author. The test program has been dedicated to deformation behavior of tensile concrete. The tests were performed in the structural laboratory of Vilnius Gediminas Technical University (VGTU) in 1993. Several innovative modifications of the test setup were made for solving problems related with noticeable limitations of the

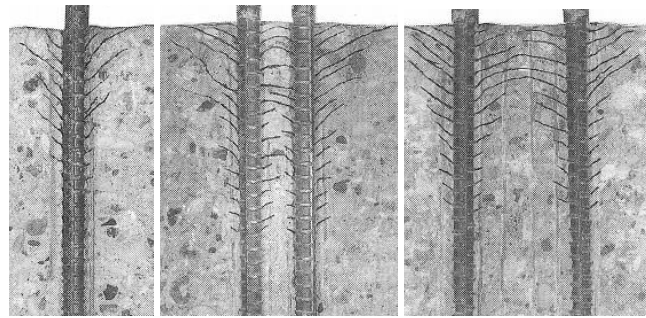
equipment existed in that period. New devices designed by R. Kupliauskas have also been employed in the tests. A uniform distribution of the tensile stresses in concrete subjected to tension load was considered as the governing condition for developing the setup. This seemingly trivial problem is closely related with different nature of the geometric and physical eccentricity in RC prisms.

Precise producing and testing of the elements might solve the geometrical eccentricity problem. The minimum loading speed of the existed tensile machine, however, was too high for identifying the cracking behavior of the RC ties and was unacceptable for testing plain concrete specimens. Thus, a new system of two speed-reducers, each with $40 \times$ capacity, and steel stiffeners (Fig. 6(a)) was developed. The series connection of the reducers has decreased the loading speed by 1600 times; the engine vibrations were prevented with a damping system. The modified loading scheme has enabled varying the loading velocity from 0.003 mm/min to 0.070 mm/min. It also ensured precise application of the tensile load eliminating a sudden release of the deformation energy related with the transverse cracks opening. Additional spherical hinges (Fig. 6(c)) were introduced for reducing the eccentricity effects. After the modification (Figs. 6(a) and 6(b)), however, the length of the test prisms became limited to 700 mm that has predetermined geometry of the test specimens. New forms have been designed and produced. These forms enabled producing specimens with different (square and circular) cross-sections. Extremities of the specimens were widened, leaving the central part for detail investigation. A distribution device (screw holder with conical hole) schematically shown in Fig. 6(c) has been developed for ensuring the central position of the reinforcement bar.

Another important aspect (the physical eccentricity) is related with the structure imperfections mentioned in the previous section. Since these imperfections are inherent to the concrete structure, the physical eccentricity could not be avoided during the tests. The eccentricity increases with the cracking (Van Mier and Van Vliet 2003). Moreover, the eccentricity magnitude varies with load (changing the crack pattern). So, the effects related with the physical eccentricity must be identified and monitored for adequate interpretation of the test outcomes. In the considered case,

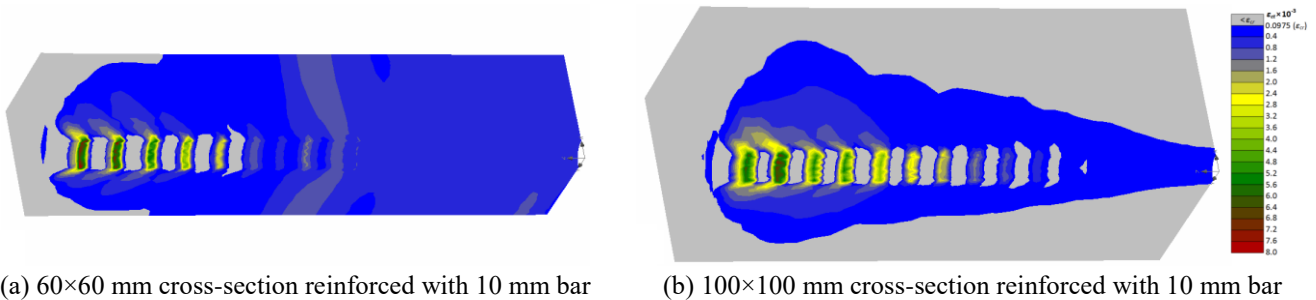


(a) Test result reported by Broms and Lutz (1965)



(b) Crack patterns around 22 mm bars spaced at different distances (Otsuka and Ozaka 1992)

Fig. 4 Effect of the bar arrangement on the crack pattern



(a) 60×60 mm cross-section reinforced with 10 mm bar

(b) 100×100 mm cross-section reinforced with 10 mm bar

Fig. 5 Modelling results by FE software ATENA of 280 mm external segments of RC ties tested by *Gribniak et al.* (2017): the results are shown only for the concrete; strains below the theoretical cracking limit are shown in grey; the stress distribution corresponds to average strain of the reinforcement equal to 0.77‰

the eccentricity effects were monitored assessing the concrete surface strains on all sides of the test specimens. The strain gauges 50 mm long attached at eight different zones of surface of the central part of the specimens were used for this purpose. The monitoring layout can be observed in Fig. 6(a), while detail description of the testing procedure is presented in Section 2.2. Such important modification enabled application of these test results for tailoring and validation of the numerical model suitable for the scatter analysis in this study.

Special geometry of the test specimens is also worth to be noted. The considered specimens represent a modification of the “dog-bone” shaped specimens for tests of the plain concrete. They, however, are also suitable for investigation of the serviceability properties (i.e., cracking and deformations) of RC elements. Unlike traditional tensile tests with the load applied to a single reinforcing bar, the shape of the considered specimens was chosen to represent the deformation behavior of a real structural member, when the load is transmitted to entire RC section. In other words, the tensile load is applied to the reinforcement bar indirectly through the surrounding concrete. Such testing layout allows eliminating the influence of end effects in RC ties. Although this method complicates deformation measurements of the reinforcement, *Gribniak et al.* (2017) demonstrated that such geometry of the ties is representative to analysis of the serviceability problems. Important advantage of such

testing layout could be also related with the ability of testing concrete elements reinforced with several bars.

Numerous devices have been employed during the tests for control of deformations and cracking behavior of the RC ties. Such instrumentation enabled a cross-verification of the test outcomes. However, a signal synchronization problem had appeared by owning a large number of the employed devices (more than 60 sensors were utilized each time). The solution was based on adapting an innovative equipment constructed in VGTU which enabled synchronization of up to 100 devices. The application of this equipment has allowed to correlate signals received from different sources during the loading process, while a personal computer was used acquiring and processing of the test readings. A graphical plotter was applied for immediate identification of appearance of the extraordinary signals. These devices are shown in Fig. 7 along to the equipped test specimen placed in the testing machine.

The considered experimental program comprised of three series of specimens. Each of the series was consisted of eight ties of three types. The elements of the first type were made of plain concrete. The specimens of second type were reinforced with a single 5 mm bar, whereas four 5 mm bars reinforced the cross-section of the third type. The bars were made of cold worked steel. In addition, four specimens with a circular shape of cross-section have been produced. In total, 28 specimens were casted with the different arrangement of the bars and shape of the cross-

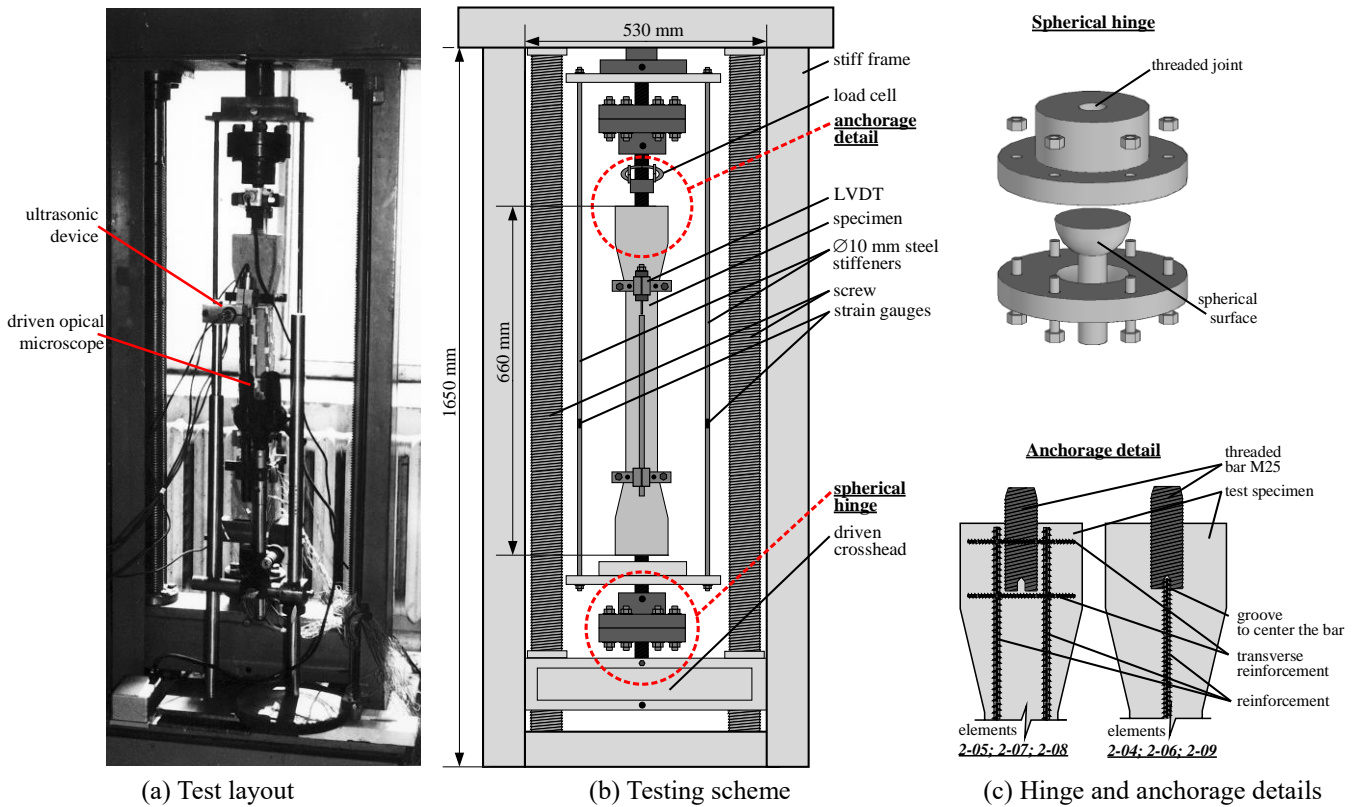


Fig. 6 Test setup

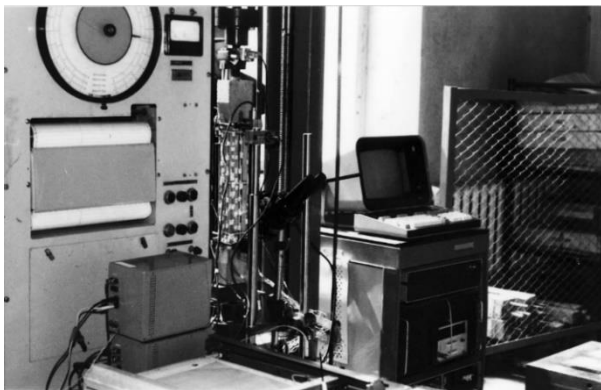


Fig. 7 Test equipped with a graphical plotter, synchronization device, and personal computer



Fig. 8 Series of the test specimens

section (rectangular and circular). All specimens are shown in Fig. 8. Producing the ties with circular (Fig. 9) section was associated with problems due to shrinkage restrained by cylindrical forms. Detail description of the shrinkage effect can be find in reference (Gribniak *et al.* 2013b). That effect has resulted in premature failure of the specimens (due to cracks localized near the extremities). Thus, the cylindrical ties were not mechanically loaded.

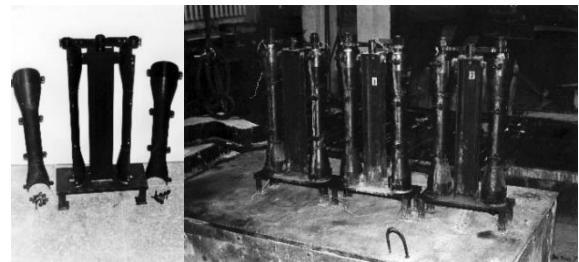


Fig. 9 Cylindrical ties: Forms and specimens

This study employs the test results of six ties with the square 60×60 mm cross-section. To evaluate arrangement effect of the bars on scatter of the test results (deformations of the concrete surface), two groups of identical ties reinforced with one and four 5 mm bars were chosen. The following specimens (Fig. 8) were selected for the analysis: the ties 2-04, 2-06, and 2-09 reinforced with one bars, and the ties 2-05, 2-07, and 2-08 reinforced with four bars.

2.1 Description of the analyzed test specimens

The specimens selected for the analysis were cast in one batch using steel forms shown in Fig. 10. This figure also provides a view of the cast specimens. The specimens were cured under laboratory conditions at average relative humidity 65% and average temperature 20°C. The RC ties were tested 180 days after the casting.

2.1.1 Concrete

The specimens were produced in one batch. Crushed granite aggregates were used. Proportions of the concrete

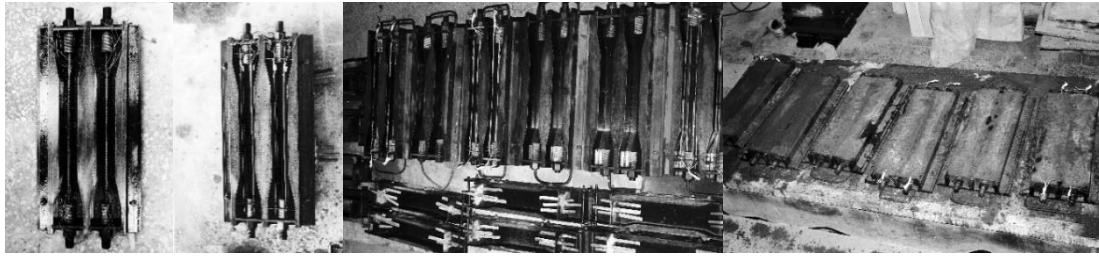


Fig. 10 Square prisms employed in this study: Forms before and after the pouring

Table 1 Mix proportion of the concrete

| Material | (kg/m ³) |
|-----------------------------------|----------------------|
| Sand 0.14/2.5 mm | 650 |
| Crushed granite aggregate 5/20 mm | 1042 |
| Cement Cem I 42.5 N | 540 |
| Water | 255 |

Table 2 Physical and mechanical properties of the concrete

| Parameter* | Value |
|--|-----------------------|
| Compressive strength at 28 day | 40.72 MPa |
| Compressive strength at the test day | 42.49 MPa |
| Tension strength at the test day | 2.89 MPa |
| Elasticity modulus at the test day | 30.12 GPa |
| Free shrinkage strain at the test day, ϵ_{cs} | -244×10^{-6} |

*The compressive strength was determined using 100 mm cubes; the elasticity modulus and the shrinkage deformations were defined for 100×100×400 mm prisms; the tension strength was defined using the standard “dog-bone” specimens with 100×100 mm cross-section

are presented in Table 1. In order to determine physical and mechanical properties of the concrete, twelve 100 mm cubes, fifteen 100×100×400 mm prisms, and standard (“dog-bone”) specimens with 100×100 mm cross-section (for tensile tests) were produced contemporarily with the RC specimens. The compressive strength was assessed two times: at the test day and at the age of 28 days. Three cubes and three prisms were tested at each age. The prisms were also used for determining shrinkage of the concrete. The obtained properties of the concrete are listed in Table 2.

2.1.2 Reinforcement

Cold worked 5 mm wire was used as the reinforcement. Three samples were tested for characterization of mechanical parameters, while several lengths were weighed for identifying the nominal diameter. The stresses and modulus of elasticity are based on the nominal dimensions. The yield strength and modulus of elasticity of the reinforcement were found equal to 527 MPa and 170 GPa, respectively.

2.1.3 Tests of RC elements

The selected ties were nominally 660 mm long; the central 350 mm part had the square 60×60 mm cross-section, whereas the ends were widened (Fig. 11(a)). All ties were reinforced with 5 mm bars. The sections were

reinforced either with one or four bars. Strain gauges attached to the reinforcement bars were used for monitoring the deformation behavior in the anchorage zones. The experimental setup is shown in Figs. 6(a) and 6(b). The spherical hinges (located at both extremities of the test specimen) were used preventing parasitic bending effects due to an eccentric tension. External strips made of steel were used for redistributing (compensating) the load drop during formation of the cracks. The center position of the reinforced bar was ensured by using screw holder (treaded bar) with conical hole shown in Fig. 6(c). For specimens with several bars, the longitudinal bars were overlapped with the treaded bar and fixed at the center position with the help of transverse reinforcement (Fig. 6(c)).

The tensile tests were carried out using an electro-mechanical loading machine of 50 kN capacity. The tests were carried out in a displacement control manner with the initial loading rate of 0.01 mm/min. During the crack formation stage the loading speed was reduced to 0.05 mm/min. Afterward, this velocity was maintained constant until the end of the test. For monitoring the applied load, a load cell (Fig. 6(b)) was used. Surface strains in the central part of the specimens were measured by means of 50 mm strain gauges at eight different levels as shown in Figs. 11(b) and 11(c). The similar strain gauges were applied for monitoring the deformations of the external bars (stiffeners) shown in Fig. 6(b). The average deformations of the concrete were also measured using linear variable deformation transducers (Fig. 11(d)). An optical microscope (with 56×magnification) and ultrasonic device indicated in Fig. 6(a) were used for labelling the crack formation process.

2.2 Results of the tensile test

As mentioned in the introduction, this study is focused to analysis of the scatter of mechanical characteristics of RC ties, which could be related with the material heterogeneity and different arrangement of the reinforcement. Rimkus *et al.* (2017) demonstrated that differences in the crack spacing are dependent on the cover depth. The surface deformations of the concrete were identified as the most important parameter revealing different deformation behavior of RC elements with different arrangement of the reinforcement. This study, therefore, considers the deformation monitoring results obtained with the help of strain gauges shown in Fig. 11.

Fig. 12 shows the deformation results of two selected specimens (i.e., the ties 2-09 and 2-08). Figs. 12(a) and

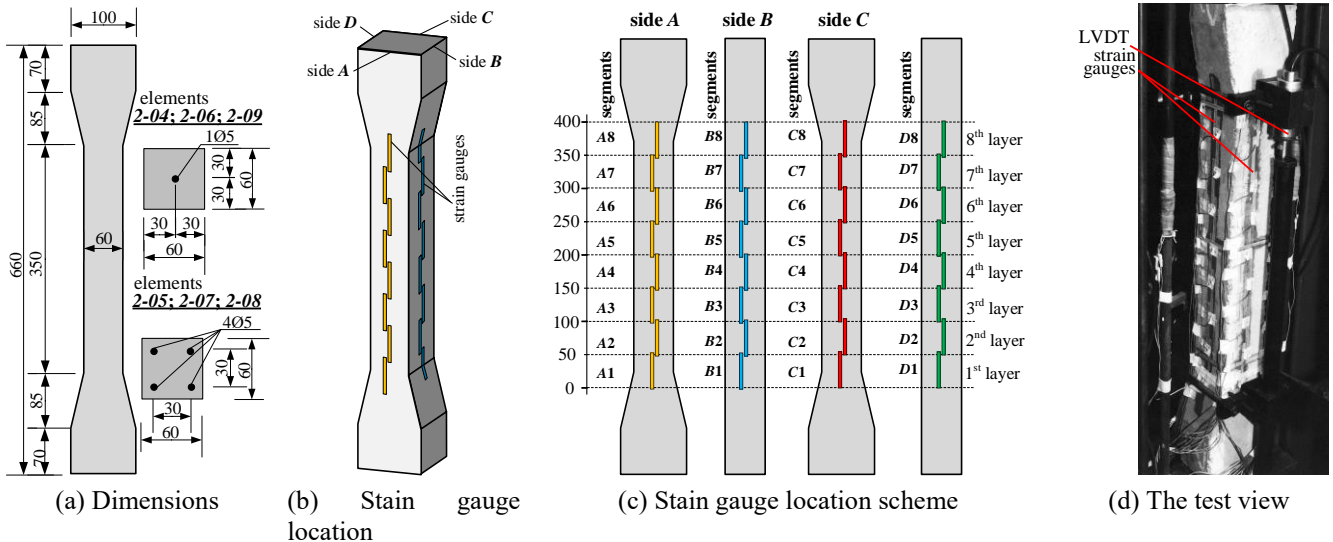


Fig. 11 Geometry of the test elements and measurement of the surface deformations

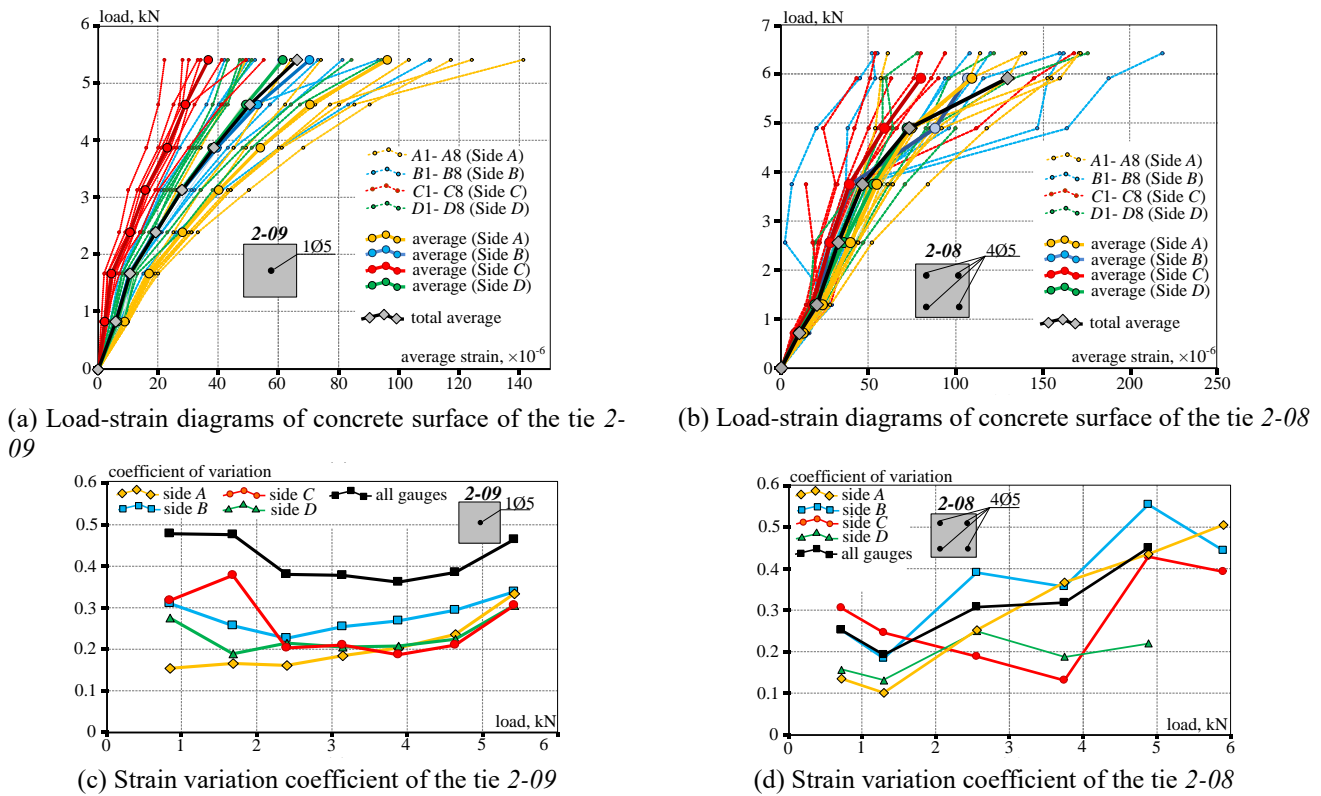


Fig. 12 Experimental results of the specimens 2-09 and 2-08

12(b) show the load-strain diagrams related to particular surfaces of the ties (see Fig. 11 for the reference): thin dashed blue lines represent the diagrams obtained using the monitoring results of the strain gauges attached to the surface A, dashed yellow – the surface B, dashed green – the surface C, and dashed red – the surface D. The graphs also include the averaged diagrams (of each surface and entire element as well). The thick solid lines (of the same color as the dashed diagrams) represent the average strain values of the surfaces, while the black lines correspond to the averaged values of all strain gauges. It is evident from

Figs. 12(a) and 12(b) that the pouring position has significant effect on the local stiffness of the concrete. The stiffest behavior is characteristic of the surface C that corresponds to the bottom of the specimens during the pouring process. The opposite side (the surface A) possesses the highest deformations. This effect is particularly apparent in specimen 2-09 reinforced with a center bar. This output is in a good agreement with results reported in the literature (Chiaia *et al.* 1998, Man and Van Mier 2011). It is known, that the bottom part of a concrete element has a more compacted structure than the top part of the specimen. That

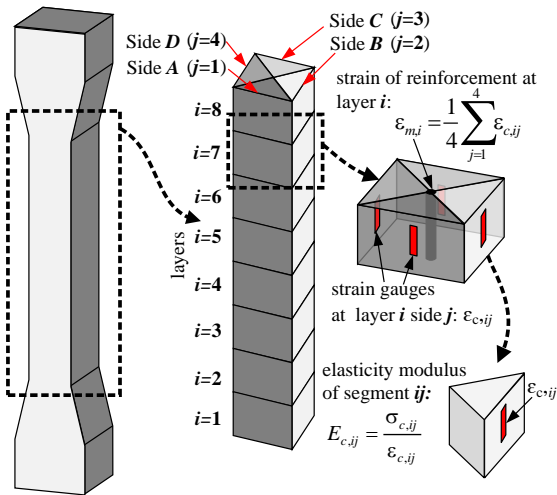


Fig. 13 Prismatic segments model

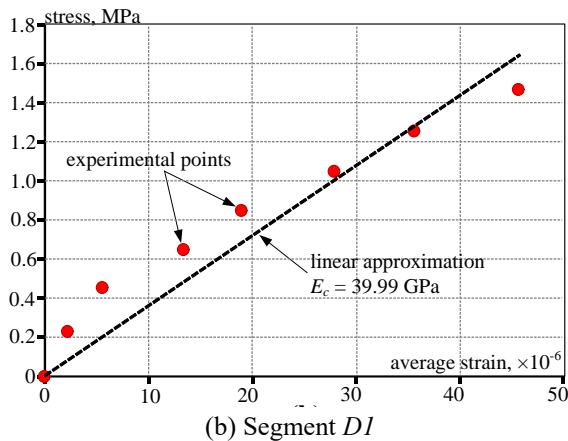
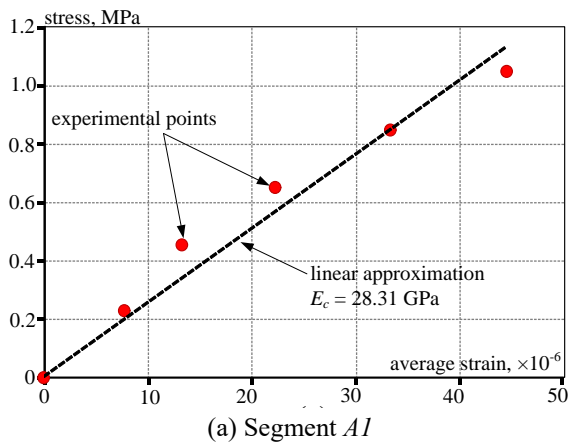


Fig. 14 Elasticity modulus assessment example of the element 2-08 (see Fig. 11 for the reference)

is a consequence of gravity effects on rough aggregates during the vibration process.

Scatter of the deformation results is another aspect that is requiring a clarification. A significant variation of the load-strain diagrams is characteristic of all surfaces at each loading stage shown in Figs. 12(a) and 12(b). However, the most noticeable scatter could be related with deformations of the tie reinforced with four bars obtained at more advanced loading stages (Fig. 12b). Figs. 12(c) and 12(d)

show the variation coefficients corresponding to the load-strain diagrams given in Figs. 12(a) and 12(b). These coefficients were determined separately for each side of the specimens as a function of the loading. The variation coefficients were also defined using outputs of all gauges (black solid lines in Figs. 12(c) and 12(d)). It can be observed that the variations assessed separately for each of the surfaces of the specimen 2-09 (reinforced with a center bar) vary in the 0.15-0.30 interval and are practically independent to the load. However, the partial variation coefficients (determined separately for each specimen side) are significantly lower than the variation coefficient defined using all monitoring results. This proves the aforementioned hypothesis about dependency of deformation behavior of the specimen surfaces on the pouring position. An opposite tendency is characteristic of the specimen 2-08 (reinforced with four bars). The scatter of the deformation monitoring results, noticeably increasing with load (up to 0.40-0.50), has the same magnitude independently whether separate surface or entire data sets are used for the analysis. Such outcome reveals more uniform deformation behavior of the concrete in the element reinforced with four bars. In the next section, a numerical simulation approach is employed to analyze this effect.

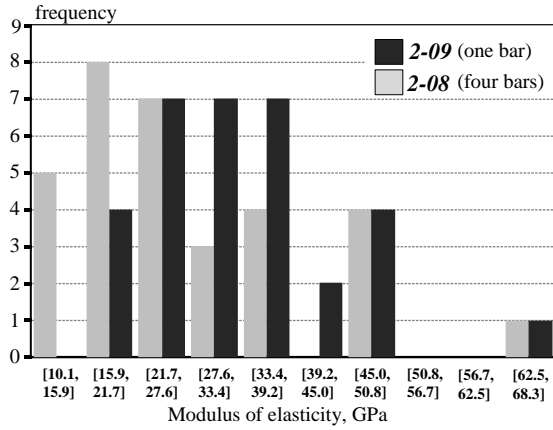
3. Numerical approach

3.1 Constitutive modeling

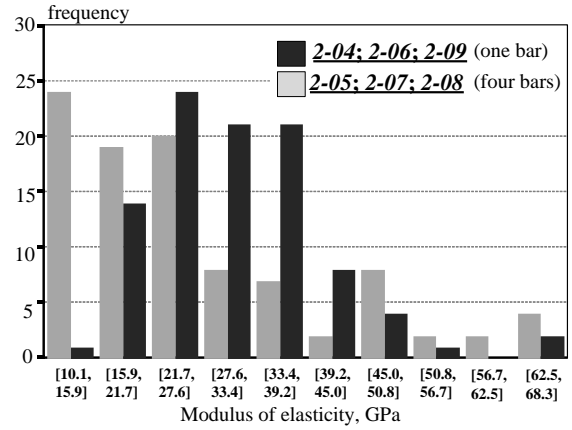
As it has been described in the previous sections, heterogeneous deformational properties of the concrete in combination with the development of internal defects inevitably causes eccentricity of the applied tensile load; the parasitic bending moments appear even using spherical hinges for transferring the load. To model the observed uneven distribution of mechanical properties of the concrete, the internal (thinned) part of the specimen is divided into eight transversal layers (corresponding the arrangement of the strain gauges in Fig. 11); four triangular prism segments compose each of the layers as shown in Fig. 13. As a result, 32 prismatic segments are represented the specimen as shown in Fig. 13(a). Deformational behavior of each external surface of the specimen is associated to the monitoring output of particular strain gauge (that was attached to this surface during the tensile test). Consequently, the 32 monitoring points are associated with the particular prismatic segments. The average stress in concrete is defined under assumption of equivalency of strains of the reinforcement and concrete in a particular transversal layer. It is also assumed that the average stress in the concrete is the same in all four prismatic segments, which compose the longitudinal layer of the specimen (Fig. 13(b)). The stress in the concrete, belonging to i -th layer, is calculated as

$$\sigma_{cm,i} = \frac{P - \epsilon_{m,i} E_s A_s}{A_c}, \quad (1)$$

where $\sigma_{cm,i}$ is the average stress in the i -th transversal layer of the concrete; $\epsilon_{m,i}$ is the average strain of the i -th segment



(a) Diagrams of two elements (2-09 and 2-08)



(b) Diagrams of six elements (the ties 2-04, 2-06, and 2-09 reinforced with one bars, and the ties 2-05, 2-07, and 2-08 reinforced with four bars)

Fig. 15 Elasticity modulus histograms

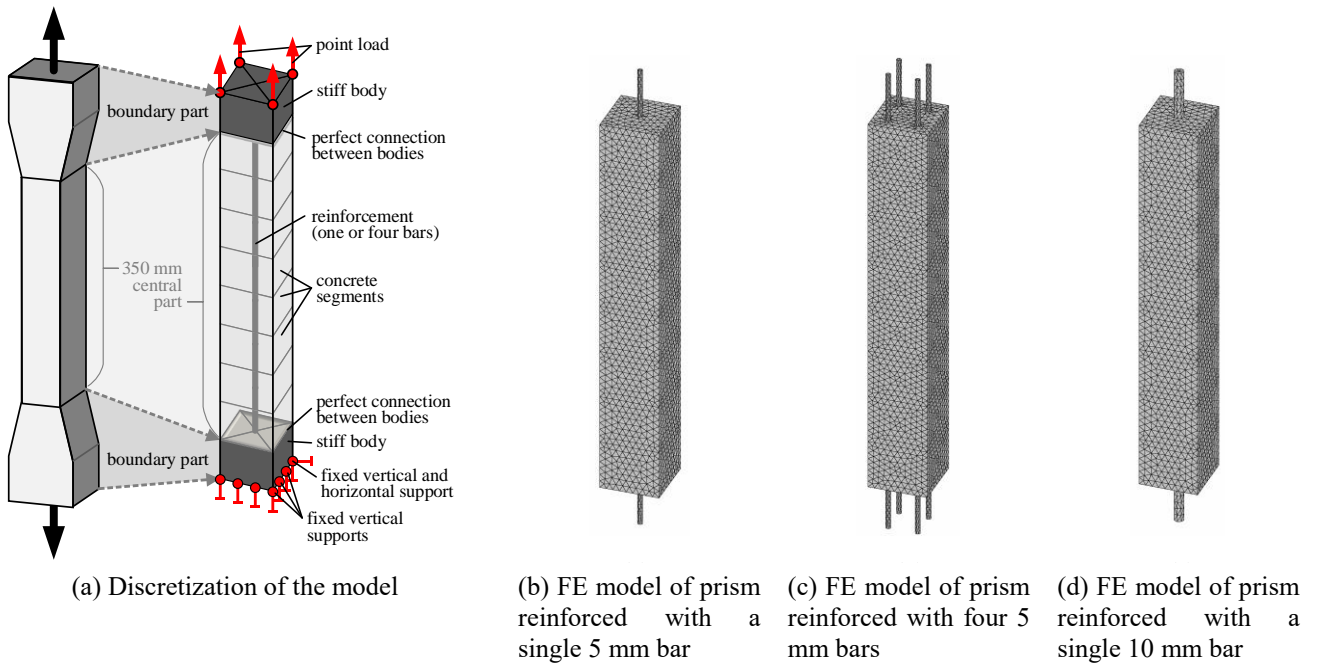


Fig. 16 Idealization of the test specimen and FE discretization of the central part of the concrete

(assessed by using results of the four strain gauges attached to surfaces of the i -th layer); E_s is the elasticity modulus of the reinforcement ($E_s=170$ GPa); A_s and A_c are the cross-section area of the reinforcement and concrete, respectively; P is the applied load (assessed by the loading cell shown in Fig. 6(b)). The elasticity modulus of the concrete belonging to the j -th prismatic segment is determined as the stress-strain ratio

$$E_{c,ij} = \frac{\sigma_{cm,i}}{\epsilon_{c,ij}}, \quad i=1\dots 8, \quad j=1\dots 4, \quad (2)$$

where $\sigma_{cm,i}$ is the average stress in concrete of the i -th transversal layer; $\epsilon_{c,ij}$ is the strain assessed using the results of strain gauge corresponding to the j -th segment (of the i -th transversal layer).

The experimental data used for the determination of elasticity modulus was limited by 40-50 micro-strains to avoid effects related with inelastic behavior of the concrete. The inelastic effects are mainly caused by development of structure defects in the considered or neighboring segments. The former case corresponds to sudden increase of the deformations (together with the elasticity modulus), while the latter case causes relaxation of deformations in the considered segment that artificially increases of the assessed deformation modulus. The elasticity moduli obtained using the test data at different loading stages were linearly approximated. Graphical illustration of this procedure for the segments $A1$ and $D1$ of the element 2-08 is shown in Fig. 14.

Fig. 15(a) shows histograms of the elasticity modulus determined for all segments of the ties considered in Fig.

12. It is evident that probability distribution of these results is far away to the normal. For the specimen 2-08 (reinforced with four bars), portion of relatively low (15-20 GPa) modulus is dominant, while the tie 2-09 (reinforced with a single bar) made of the same concrete possess an opposite outcome. The same tendency is characteristic of the histograms shown in Fig. 15(b), which include elasticity moduli determined for all specimens selected for the analysis, i.e., three specimens reinforced with a single bar (the ties 2-04, 2-06, and 2-09) and three ties reinforced with four bars (the ties 2-05, 2-07, and 2-08). Such results correlate with the test outcomes identified in Fig. 12. In opposite to the elements reinforced with a single bar, the larger number of bars ensures uniform distribution of deformations within the concrete. Higher average deformations monitored at the surface of the ties reinforced with four bars (e.g., Fig. 12(b)) result in a dominantly lower elasticity modulus of the concrete than characteristic for the ties reinforced with a single bar (Fig. 15). In the next section, the determined elasticity moduli of concrete are assigned to the corresponding regions of finite element model for representing the bar arrangement effect on the deformation behavior of the tensile elements.

3.2 Finite element analysis

Finite element (FE) software ATENA is employed to the numerical analysis (Jendele and Cervenka 2006). The deformation problem is solved in the 3D formulation using the Newton-Raphson iteration procedure. Isoparametric tetrahedral elements with 10 degrees of freedom and four integration points are used. As suggested in the reference (Mang *et al.* 2016), a relatively fine FE mesh size is used for ensuring discretization adequacy of the concrete cover (equal to 13 mm in the specimens reinforced with four bars). The average FE size is equal to 7 mm. Since detail experimental measurements were limited to the central thinned part of the specimen, only this part is used for the modelling (Fig. 16(a)). The numerical model employs the same segment discretization as used for the constitutive modelling (Section 3.1). FE models of the ties reinforced with one and four bars are shown in Figs. 16(b) and 16(c). Fig. 16(d) shows the model of a theoretical tie reinforced with a single 10 mm bar (of the same area as four 5 mm bars). To simplify the model, the outer (disregarded) parts of the specimen are modeled as stiff bodies (shown in Fig. 16(a), but hidden in Figs. 16(b)-16(d)) with idealized material properties. Uniformly distributing the applied tensile load to the extremities of the central concrete part, these bodies are perfectly bonded to the inner (analyzed) concrete prism. Fig. 16(a) specifies the boundary conditions of the model. As can be observed, four equal nodal forces are applied to the external corners of the stiff body located at the top of the modeled specimen, whereas horizontal and vertical displacements of the bottom surface of another stiff element are prevented.

For concrete, SBETA material model offered by ATENA is utilized. This model is based on the concept of smeared cracks and damage (Gribniak *et al.* 2013a). Concrete without cracks is considered as isotropic and concrete with cracks as orthotropic body. Cracking of the concrete was

modeled using the softening law proposed by Hordijk (1991). The fracture energy of the concrete G_f is assumed equal to 80 N/m. Since an exact tensile strength of the concrete within particular segments is unknown, it is assumed the same for all segments and equal to the experimentally defined strength value (2.89 MPa). The elasticity moduli of the concrete defined in Section 3.1 are assigned to the corresponding regions of the model (Fig. 16(a)). The results of the ties 2-09 and 2-08 are used for simulating prisms reinforced with one (Fig. 16(b)) and four bars (Fig. 16(c)), respectively. In this way, the simulated deformation behavior was associated with the particular monitoring results (Figs. 12(a) and 12(b)). Reinforcement is modeled as linear elastic material with the elasticity modulus E_s equal to 170 GPa using the isoparametric tetrahedral elements. Such discretization enables straightforward modelling of the tension-stiffening effect (Gribniak *et al.* 2017). The perfect bond model is used for representing contact between reinforcement and concrete. The references (Mang *et al.* 2016, Rimkus *et al.* 2017) proved adequacy of such simplified assumption for the case of a relatively small deformations (considered in this study). To investigate the bar arrangement effect on the deformation response, the theoretical model of the prism reinforced with a single 10 mm bar (Fig. 16(d)) is also considered. This model employs the same material characteristics as the model with a single 5 mm bar (Fig. 16(b)).

The calculated and experimental load-strain diagrams are compared in Fig. 17. The experimental diagrams were obtained by averaging results of all strain gauges. The numerical diagrams were determined by averaging displacements of four surfaces of the modeled prism. The maximum experimental load of the specimen 2-09 was equal to 5.86 kN (Fig. 17(a)). The test was terminated due to failure of the concrete within the widened part of the specimen. In the tie 2-08, the overlapped connection of the longitudinal reinforcement (Fig. 6(c)) has ensured sufficient strength of the widened part: the ultimate load has reached 11.75 kN. Thus, the experimental diagram shown in Fig. 17(b) reaches a more advanced loading stage.

As can be observed in Fig. 17, the initial stiffness of the experimental specimens was predicted adequately; however, the cracking load was overestimated for both specimens (solid lines in Fig. 17). Numerous investigations, e.g., (Broms and Lutz 1965, Michou *et al.* 2015, Gribniak *et al.* 2013b, 2015, 2016b), reported that restrained shrinkage of concrete might noticeably decrease of cracking resistance of RC members. In concrete elements, reinforcement bar restrains shrinkage deformations developing tensile stresses in the surrounding concrete. Prior to mechanical loading, magnitude of these stresses is governed by the reinforcement ratio. The larger the reinforcement ratio, the higher initial tensile stresses develops in the concrete. To illustrate this effect, the numerical study includes the concrete shrinkage into the consideration. For this purpose, the experimentally obtained shrinkage strain (-244×10^{-6}) is used. Prior to the mechanical loading, the total shrinkage deformation is prescribed, using 10 equal increments, to all concrete segments (Fig. 16(a)). The external load is also

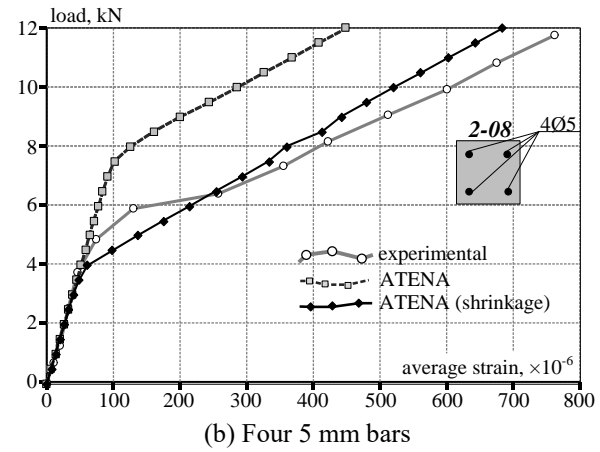
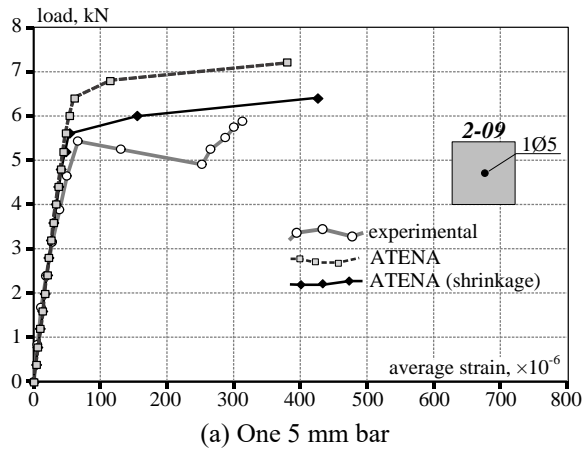


Fig. 17 Calculated and experimental load-strain diagrams of prisms with different reinforcement

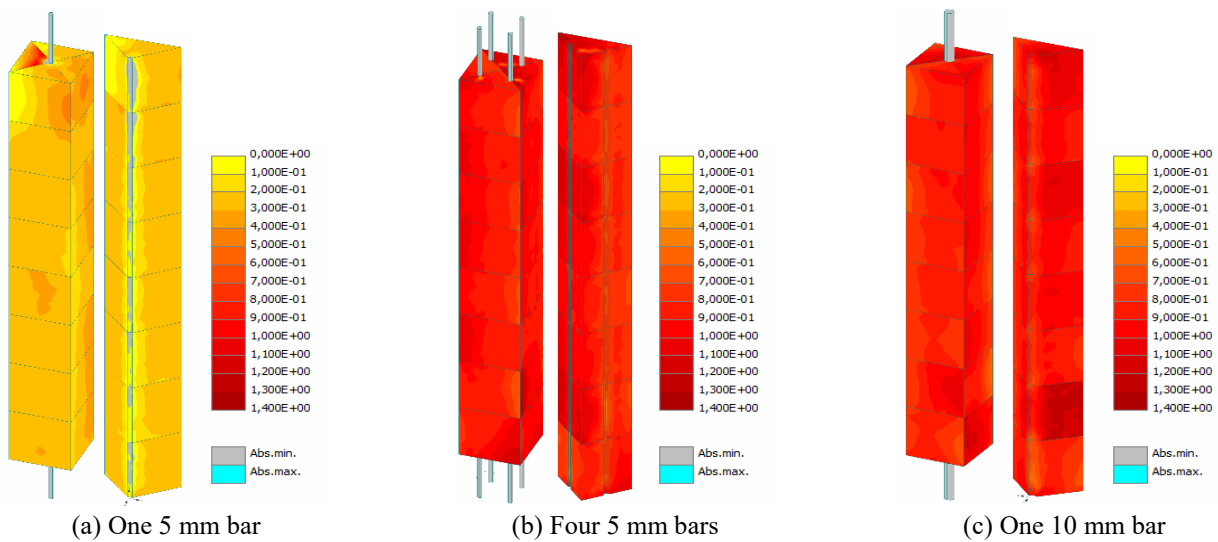


Fig. 18 Distribution of the shrinkage-induced stresses in the concrete prisms with different reinforcement

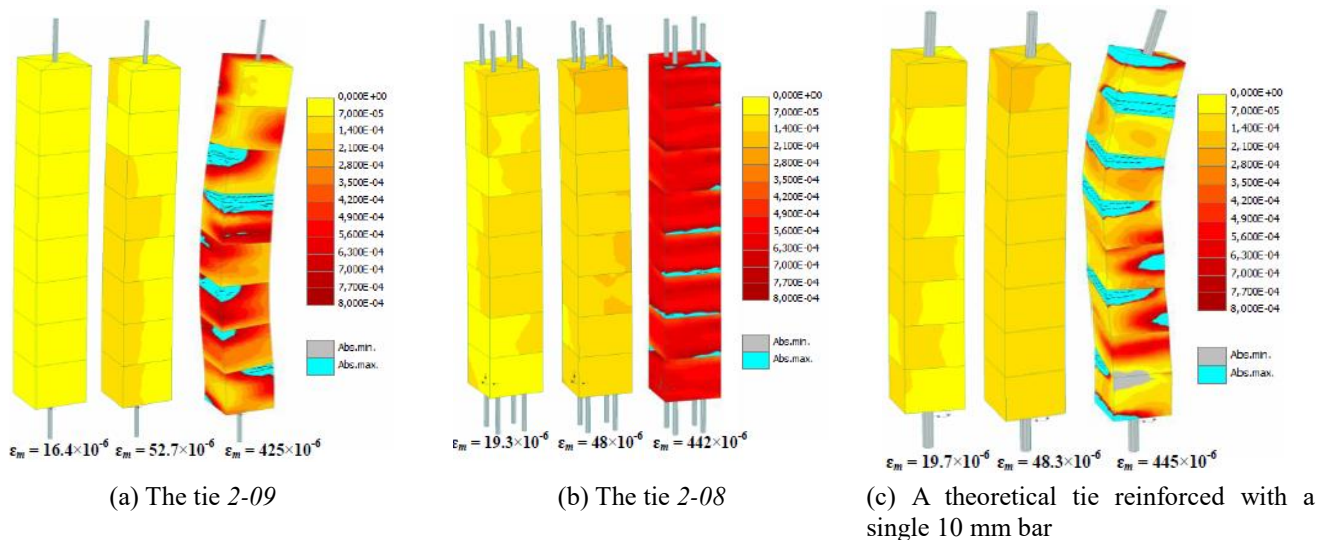


Fig. 19 Deformed shapes of the concrete prisms with different reinforcement (200×magnification scale)

applied incrementally (with the 100 N load step). The modeled load-average strain diagrams taking into account the shrinkage effect are shown in Fig. 17 (dashed lines).

The simulation results reveal prediction adequacy of both the initial stiffness and the cracking loads. Hence, the simulation results of the upgraded model (including the

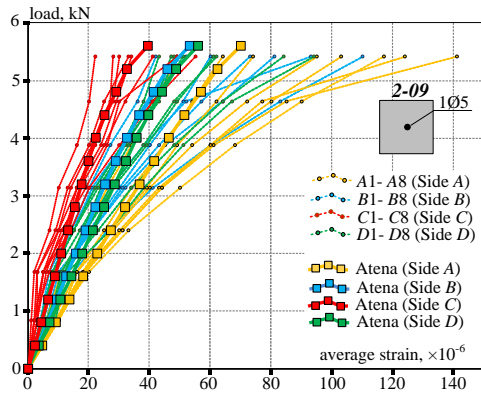


Fig. 20 Simulated and experimental load-strain diagrams of different surfaces of the specimen 2-09

shrinkage effect) is used for the deformation analysis.

The simulated distribution of tensile stresses in the concrete prisms owning the shrinkage released prior to the mechanical loading is shown in Fig. 18. This figure includes views of the quarter-segments, which demonstrate internal distribution of the strains in concrete. Fig. 18 also includes simulation results of the theoretical prism reinforced with a single 10 mm bar (Fig. 16(d)). The shrinkage-induced stresses in the concrete reach up to 1.4 MPa that corresponds to 50% of the tensile strength of the concrete (Table 2). It is evident that such stresses accumulated within the concrete at the pre-loading stage lead by significant reduction of the cracking load. This effect is more significant in specimens with higher amount of the reinforcement. In the considered cases, the reinforcement ratio of the prism reinforced with a single 5 mm bar (Fig. 18(a)) is equal to 0.54%, while the remaining two specimens (Figs. 18(b) and 18(c)) have the reinforcement ratio equal to 2.18%. Fig. 18(a) reveals that the tensile stresses in the concrete are localized around the reinforcement bar. An increase of the reinforcement area makes distribution of the stresses within the concrete more uniform (Figs. 18(b) and 18(c)). Fig. 18 also indicates that elasticity modulus variation causes non-uniform stress distribution in the concrete segments: higher modulus of elasticity induces higher tensile stresses.

Fig. 19 shows the deformed shapes of the specimens with different reinforcement. The presented modeling results are related with similar magnitudes of average deformation of the reinforcement, ε_m . The figure also indicates strain distribution in the concrete. Strain value of 0.8% was assumed as the boundary (sky-blue filling indicates the regions in Fig. 19 where the strains exceed the boundary value). Referring to the assumed FE size (≈ 7 mm), the boundary value indicates location of visible cracks (Mang *et al.* 2016). The ultimate strain regions are evidently localized in boundary zones of the concrete segments, which could be related with uneven distribution of the elasticity modulus. The differences in deformation properties generate a parasitic curvature within the tensile specimen even at low loading stages. This effect is particularly evident in the prisms reinforced with a single bar (Figs. 19(a) and 19(c)), while a larger number of the

bars reduces effects associated with the heterogeneity of the concrete. It must be pointed out, however, that these results could be attributed to the idealized numerical model.

Fig. 20 shows the load-strain diagrams of the prism 2-09 (reinforced with a single 5 mm bar). The simulated diagrams are shown separately for each side of the specimen. Although the simulated stiffness of the side A (the top surface during the pouring of the concrete) is noticeably lower in comparison to the side C (the bottom pouring surface), the test results possess much more significant diversities than the numerical assessments. Such disagreement could be related with physical aspects more complex than the simplified assumptions of the presented numerical model. The local tensile strength of the cement matrix could be mentioned as one of the most important characteristics of the concrete. However, it was remained outside of the scope of the test program taken as the base for the presented analysis. Further research is necessary to investigate this effect.

Results of this study are in good agreement with the previous findings (Gribniak *et al.* 2017, 2018), supporting the general inference about non-linearity of strain gradient in the tensile concrete. The end effect is characteristic of the traditional tensile tests when tensile load is transferred through the bond of the bar reinforcement. This effect increases with the cover depth. Application of the special geometry of tensile specimens might solve this problem (Fig. 19). However, a noticeable extent of the parasitic curvatures in the prisms reinforced with a single bar reveals important limitation of such reinforcement scheme (Figs. 19(a) and 19(c)). Prisms reinforced with multiple bars demonstrate a more stable deformation response (Fig. 19(b)). Such arrangement of the reinforcement reduces stochastic deformation component related with heterogeneity of structure of the concrete. Notwithstanding ability of FE software of simulating adequate deformation behavior of all considered tensile elements, specimens reinforced with multiple bars are recommended as the object for characterizing mechanical properties of reinforced concrete.

4. Conclusions

Structure of concrete can be considered as a combination of components with different mechanical characteristics and interaction mechanisms. The heterogeneous structure leads to different mechanical properties of the concrete in different loading situations. It could be attributed to a low resistance of the cement matrix to development of the tension cracks. In practical applications, the tension zone of concrete elements is reinforced for compensating the low cracking resistance. In the presence of bar reinforcement, however, development of the cracks becomes even more complicated due to appearance of a new structure component – the interaction zone between the concrete and reinforcement. The direct tension test is the most widely used layout for analyzing mechanical properties of the reinforced concrete.

This study is dedicated to analysis of the scatter of the test results that could be related with arrangement of bar

reinforcement. The study is based on the tests performed in the structural laboratory of Vilnius Gediminas Technical University in 1993: 28 concrete specimens with different arrangement of the bars and shape of the cross-section (rectangular and circular) were subjected to short-term tension. Several innovative modifications of the test setup were made for solving problems related with noticeable limitations of the equipment available in the last decade of the past century. A uniform distribution of tensile stresses in the concrete was the aim of the modification. This problem seems trivial, but the actual complexity is related with different nature of the geometric and physical eccentricity in reinforced concrete tensile elements. Precise producing and testing the specimens might solve problems related with the geometrical eccentricity. The physical eccentricity, however, is related with structure imperfections of the concrete. Since these imperfections are inherent to structure of the concrete, the corresponding effects must be accounted for adequate interpretation of the test outcomes. In the considered test program, it was done by monitoring surface strains of the concrete. Strain gauges attached along each surface of the concrete specimen were used for this purpose. Special geometry of the test specimens is worth to be noted. It represents a modification of the “dog-bone” shaped specimen for tests of the plain concrete. Unlike traditional tensile tests with the load applied to a single reinforcing bar, the tensile load is applied to the reinforcement bar indirectly through the surrounding concrete. Important advantage of such testing layout could be also related with the ability of composing concrete sections reinforced with several bars.

This study has employed the test results of six elements with square 60×60 mm cross-section in the monitoring zone. To evaluate the arrangement effect of the reinforcement, two groups of the ties reinforced with one and four 5 mm bars were considered. The monitored part of the specimen was divided into eight transversal layers; four triangular prisms composed each of them. Deformational behavior of each external surface of the specimen was associated to the monitoring output of particular strain gauge. Average stress in concrete was defined under assumption of equivalency of strains of the reinforcement and concrete in the segment. The average stresses in all four prismatic segments of the transversal layer of the concrete were also assumed the same. The elasticity modulus of the concrete belonging to particular prismatic segment was determined as the stress-strain ratio (using the results of the corresponding strain gauge).

It is important to note that all specimens were made of the same concrete. For the specimens reinforced with four bars, however, portion of relatively low (10-22 GPa) elasticity modulus was dominant, while the prisms reinforced with a single bar possess an opposite outcome: the modulus of 22-40 GPa were prevailing. (The experimentally determined elasticity modulus was equal to 30.1 GPa.) The variation analysis has proved dependency of deformation characteristics of the specimen surfaces on the pouring position in the elements reinforced with a center bar. Another tendency is characteristic of the specimen reinforced with four bars: the deformation behavior was practically independent on the pouring layout. These outcomes reveal diversity of deformation behavior of the concrete with different arrangement of reinforcement bars.

Deformation behavior of the ties was analyzed by applying FE approach. Since an exact tensile strength of the concrete within particular segments is unknown, it was assumed the same for all segments and equal to the experimentally defined strength value. The identified elasticity moduli of the concrete were assigned to the corresponding regions of FE model. Unlike the common practice, the shrinkage effect realized at the pre-loading stage was accounted. The assessed shrinkage-induced stresses in the concrete have reached up to 1.4 MPa that corresponds to 50% of the experimentally determined tensile strength of the concrete. It is evident that the accumulation of such stresses reduces the cracking resistance of the element.

The numerical simulations have revealed the effects, which were neglected during the test results interpretation stage. The differences in deformation properties of the concrete segments generated a parasitic curvature within the tensile specimen even at low loading stages. This effect was particularly evident in the prisms reinforced with a single bar, while a larger number of the bars reduced effects associated with the heterogeneity of the concrete. However, it must be pointed out that these results are related to a simplified numerical model. Although the simulated stiffness of the top surface of the concrete pouring was noticeably lower in comparison to the bottom surface of pouring, the test results possessed much more significant diversities than the numerical assessments. The further studies must address the effects related with the local tensile strength of the cement matrix, which have remained outside of the scope of the experimental program taken as the base for this study. The reported results, however, indicate that the application of multiple bar reinforcement might reduce the stochastic deformation component related with heterogeneity of structure of the concrete. The elements with multiple arrangement of reinforcement bars are recommended as the object for characterizing mechanical properties of reinforced concrete.

Acknowledgments

The authors gratefully acknowledge the financial support provided by the Research Council of Lithuania (Research Project S-MIP-17-62).

References

- Beeby, A.W. (1978), “Corrosion of reinforcing steel in concrete and its relation to cracking”, *Struct. Eng.*, **56**(3), 77-81.
- Borosnyói, A. and Snóbli, I. (2010), “Crack width variation within the concrete cover of reinforced concrete members”, *Éptóanyag-J. Silic. Bas. Compos. Mater.*, **62**(3), 70-74.
- Broms, B.B. (1965), “Crack width and crack spacing in reinforced concrete members”, *ACI J. Proc.*, **62**(10), 1237-1256.
- Broms, B.B. and Lutz L.A. (1965), “Effects of arrangement of reinforcement on crack width and spacing of reinforced concrete members”, *ACI J. Proc.*, **62**(11), 1395-1410.
- Caduff, D. and Van Mier, J.G.M. (2010), “Analysis of compressive fracture of three different concretes by means of 3D-digital image correlation and vacuum impregnation”, *Cement Concrete Compos.*, **32**(4), 281-290.
- Caldentey, A.P., Peiretti, H.C., Iribarren, J.P. and Soto, A.G.

- (2013), "Cracking of RC members revisited: influence of cover, ϕ_{eff} and stirrup spacing – an experimental and theoretical study", *Struct. Concrete*, **14**(1), 69-78.
- Chen, Z., Xu, J., Chen, Y. and Su, Y. (2016), "Seismic behavior of T-shaped steel reinforced high strength concrete short-limb shear walls under low cyclic reversed loading", *Struct. Eng. Mech.*, **57**(4), 681-701.
- Chiaia, B., Van Mier, J.G.M. and Vervuurt, A. (1998), "Crack growth mechanisms in four different concretes: Microscopic observations and fractal analysis", *Cement Concrete Res.*, **28**(1), 103-114.
- Clark, A.P. (1946), "Comparative bond efficiency of deformed concrete reinforcing bars", *ACI J. Proc.*, **43**(11), 381-400.
- Diamond, S. (2004), "The microstructure of cement paste and concrete – a visual primer", *Cement Concrete Compos.*, **26**(8), 919-933.
- Elaqra, H., Godin, N., Peix, G., R'Mili, M. and Fantozzi, G. (2007), "Damage evolution analysis in mortar, during compressive loading using acoustic emission and X-ray tomography: Effects of the sand/cement ratio", *Cement Concrete Res.*, **37**(5), 703-713.
- Goto, Y. (1971), "Cracks formed in concrete around deformed tension bars", *ACI J. Proc.*, **68**(4), 244-251.
- Gribniak, V., Caldentey, A.P., Kaklauskas, G., Rimkus, A. and Sokolov, A. (2016a), "Effect of arrangement of tensile reinforcement on flexural stiffness and cracking", *Eng. Struct.*, **124**, 418-428.
- Gribniak, V., Cervenka, V. and Kaklauskas, G. (2013a), "Deflection prediction of reinforced concrete beams by design codes and computer simulation", *Eng. Struct.*, **56**, 2175-2186.
- Gribniak, V., Jakubovskis, R., Rimkus, A., Ng, P.-L. and Hui, D. (2018), "Experimental and numerical analysis of strain gradient in tensile concrete prisms reinforced with multiple bars", *Constr. Build. Mater.*, **187**, 572-583.
- Gribniak, V., Kaklauskas, G., Kliukas, R. and Jakubovskis, R. (2013b), "Shrinkage effect on short-term deformation behavior of reinforced concrete – when it should not be neglected", *Mater. Des.*, **51**, 1060-1070.
- Gribniak, V., Mang, H.A., Kupliauskas, R. and Kaklauskas, G. (2015), "Stochastic tension-stiffening approach for the solution of serviceability problems in reinforced concrete: Constitutive modelling", *Comput.-Aid. Civil Infrastruct. Eng.*, **30**(9), 684-702.
- Gribniak, V., Mang, H.A., Kupliauskas, R., Kaklauskas, G. and Juozapaitis, A. (2016b), "Stochastic tension-stiffening approach for the solution of serviceability problems in reinforced concrete: Exploration of predictive capacity", *Comput.-Aid. Civil Infrastruct. Eng.*, **31**(6), 416-431.
- Gribniak, V., Rimkus, A., Torres, L. and Jakstaite, R. (2017), "Deformation analysis of RC ties: Representative geometry", *Struct. Concrete*, **18**(4), 634-647.
- Gudonis, E., Rimkus, A., Kaklauskas, G., Gribniak, V. and Kupliauskas, R. (2014), "Experimental investigation on deformation behavior of RC ties", *Proceedings of the 19th International Conference Mechanika*, Kaunas, Lithuania.
- Hordijk, D.A. (1991), "Local approach to fatigue of concrete", Ph.D. Dissertation, Delft University of Technology, Delft, the Netherlands.
- Hwang, L.S. (1983), "Behaviour of reinforced concrete in tension at post-cracking range", M.Sc. Dissertation, University of Manitoba, Winnipeg, Canada.
- Ingaffea, A.R., Gerstle, W.H., Gergely, P. and Saouma, V. (1984), "Fracture mechanics of bond in reinforced concrete", *J. Struct. Eng.*, **110**(4), 871-890.
- Jakubovskis, R., Kaklauskas, G., Gribniak, V., Weber, A. and Juknys, M. (2014), "Serviceability analysis of concrete beams with different arrangement of GFRP bars in the tensile zone", *J. Compos. Constr.*, **18**, Paper ID: 04014005.
- Jendele, L. and Cervenka, J. (2006), "Finite element modelling of reinforcement with bond", *Comput. Struct.*, **84**(28), 1780-1791.
- Lee, G.Y. and Kim, W. (2009), "Cracking and tension stiffening behavior of high-strength concrete tension members subjected to axial load", *Adv. Struct. Eng.*, **12**(2), 127-137.
- Man, H.K. and Van Mier, J.G.M. (2011), "Damage distribution and size effect in numerical concrete from lattice analyses", *Cement Concrete Compos.*, **33**(9), 867-880.
- Mang, C., Jason, L. and Davenne, L. (2016), "Crack opening estimate in reinforced concrete walls using a steel-concrete bond model", *Arch. Civil Mech. Eng.*, **16**, 422-436.
- Michou, A., Hilaire, A., Benboudjema, F., Nahas, G., Wyniecki, P. and Berthaud, Y. (2015), "Reinforcement-concrete bond behavior: Experimentation in drying conditions and meso-scale modelling", *Eng. Struct.*, **101**, 570-582.
- Otsuka, K. and Ozaka, Y. (1992), "Group effects on anchorage strength of deformed bars embedded in massive concrete block", *Proceedings of the International Conference – Bond in Concrete from Research to Practice*, Riga, Latvia.
- Patel, K.A., Chaudhary, S. and Nagpal, A.K. (2016), "A tension stiffening model for analysis of RC flexural members under service load", *Comput. Concrete*, **17**(1), 29-51.
- Prado, E.P. and Van Mier, J.G.M. (2003), "Effect of particle structure on mode I fracture process in concrete", *Eng. Fract. Mech.*, **70**(14), 1793-1807.
- Purainer, R. (2005), "Last- und verformungsverhalten von stahlbetonflächentragwerken unter zweiaxialer zugbeanspruchung", Ph.D. Dissertation, University of the Federal Armed Forces, Munich, Germany.
- Rimkus, A., Jakstaite, R., Kupliauskas, R., Torres, L. and Gribniak, V. (2017), "Experimental identification of cracking parameters of concrete ties with different reinforcement and testing layouts", *Proc. Eng.*, **172**, 930-936.
- Rostásy, F., Koch, R. and Leonhardt, F. (1976), "Zur mindestbewehrung für zwang von außenwänden aus stahlleichtbeton", *Deutscher Ausschuss für Stahlbeton*, **267**, 1-107.
- Schlangen, E. and Van Mier, J.G.M. (1992), "Experimental and numerical analysis of micro-mechanisms of fracture of cement-based composites", *Cement Concrete Compos.*, **14**(2), 105-118.
- Shiotania, T., Bisschop, J. and Van Mier, J.G.M. (2003), "Temporal and spatial development of drying shrinkage cracking in cement-based materials", *Eng. Fract. Mech.*, **70**(12), 1509-1525.
- Theiner, Y. and Hofstetter, G. (2009), "Numerical prediction of crack propagation and crack widths in concrete structures", *Eng. Struct.*, **31**(8), 1832-1840.
- Tijssens, M.G.A., Sluys, L.J. and Van der Giessen, E. (2001), "Simulation of fracture of cementitious composites with explicit modeling of micro structural features", *Eng. Fract. Mech.*, **68**(11), 1245-1263.
- Van Mier, J.G.M. (1991), "Mode I fracture of concrete: Discontinuous crack growth and crack interface grain bridging", *Cement Concrete Res.*, **21**(1), 1-15.
- Van Mier, J.G.M. and Van Vliet, M.R.A. (2003), "Influence of microstructure of concrete on size/scale effects in tensile fracture", *Eng. Fract. Mech.*, **70**(16), 2281-2306.
- Williams, A. (1986), *Test on Large Reinforced Concrete Elements Subjected to Direct Tension*, Technical Report 562, Cement and Concrete Association, Wexham Springs.